Bayesian Discovery of a Sub-Quadratic Silicon Nanobeam Cavity with Simulated Quality Factor of 24.6 Million for Quantum-Emitter Interfaces

Abhinav Nigam and Kishore Nair
Panther Creek High School
Cary, North Carolina, USA
{abhinav.nigam.902, kishoreisformal}@gmail.com

***Abstract*—Efficient solid-state quantum-network nodes require optical interfaces that direct emission from stationary quantum emitters into a selected photonic mode. We report a computational search for silicon photonic-crystal nanobeam cavities in which the taper exponent was optimized jointly with four additional geometric variables rather than fixed at the commonly used quadratic value. A checkpointed Gaussian-process Bayesian optimizer orchestrated approximately 300 three-dimensional finite-difference time-domain jobs across successive exploratory, refinement, and verification stages on TACC's Stampede3 system. Persistent checkpoints preserved the optimizer's accumulated observations across scheduler interruptions and failed jobs. The terminal focused stage was warm-started from a cavity with a simulated quality factor near 3.6 million and identified a near-linear taper exponent of 1.08276. The selected design achieved a simulated quality factor of 24.6304 million. Higher-resolution field characterization produced an estimated normalized mode volume of 0.38461 cubic wavelengths in the dielectric and a silicon electric-energy overlap of 90.762 percent. Combined with the simulated quality factor, this mode-volume estimate corresponds to an ideal Purcell-factor estimate of 4.86212 million under perfect spatial, spectral, and dipole alignment. The result identified a high-performing sub-quadratic region within the investigated five-dimensional design space and demonstrates a fault-tolerant route for coupling Bayesian photonic design search to parallel electromagnetic simulation in support of future integrated quantum-emitter interfaces.**

***Index Terms*—quantum photonics, quantum-emitter interface, photonic-crystal cavity, Bayesian optimization, Purcell enhancement, high-performance computing**

I. Introduction

Optically addressable solid-state spins and other quantum emitters can serve as stationary quantum memories or processors, while photons provide a natural channel for transmitting quantum information between nodes [1]. Their practical connection depends on directing emission into a desired optical mode rather than competing radiative and nonradiative channels. Photonic-crystal cavities reshape the local optical density of states and can enhance emission into a resonant mode when the emitter is spatially, spectrally, and polarization aligned with the cavity field [2], [3]. For a normalized mode volume $\widetilde{V} = V_{\text{eff}}/(\lambda/n)^3$, the ideal geometric Purcell estimate is

$$F_{P,\text{ideal}} = \frac{3}{4\pi^2}\frac{Q}{\widetilde{V}}, \tag{1}$$

where Q is the cavity quality factor. Equation (1) is used here as a cavity figure of merit; an experimentally attainable enhancement also depends on the emitter linewidth, detuning, position, and dipole orientation.

Widely used deterministic nanobeam designs employ a quadratic variation of lattice constant through the defect region [3]. We instead treated the taper exponent as a free coordinate in a joint five-dimensional search. The scientific objective was to identify a high-$Q/\widetilde{V}$ geometry for prospective quantum-emitter interfaces. The computational objective was to preserve optimizer state across scheduler limits, failed jobs, and repeated parallel MEEP launches.

II. Checkpointed Bayesian–FDTD Workflow

The cavity comprised a 500-nm-wide, 220-nm-thick silicon nanobeam with eight mirror holes per side and a fixed hole-radius ratio $r/a = 0.28$. For N_{def} defect intervals, the local period was generated by

$$a_i = a_{\text{start}} + (a_{\text{end}} - a_{\text{start}})\left(\frac{i}{N_{\text{def}}+1}\right)^p, \tag{2}$$

where the optimizer jointly varied a_{start}, a_{end}, taper exponent p, integer defect count N_{def}, and central spacer s_{cav}.

Successive stages used a Gaussian-process optimizer with an expected-improvement acquisition function [4]. The terminal stage narrowed the bounds to $a_{\text{start}} \in [0.41, 0.44]$ μm, $a_{\text{end}} \in [0.32, 0.35]$ μm, $p \in [0.8, 1.3]$, $N_{\text{def}} \in [4, 7]$, and $s_{\text{cav}} \in [0.13, 0.16]$ μm. It was warm-started from a previously identified $Q \approx 3.6 \times 10^6$ geometry. Across the broader development and optimization campaign, approximately 300 FDTD jobs were launched.

Each completed evaluation was passed to the optimizer, appended to a timestamped CSV file, and serialized to a checkpoint. After a scheduler interruption, the controller loaded the saved Gaussian-process state and resumed from its accumulated observations. A Bash compatibility layer purged conflicting modules, loaded MEEP 1.28 and Intel MPI, configured the OFI/TCP fabric, cleared conflicting library paths, and invoked each geometry through `ibrun` on 36 MPI ranks. Fig. 1 summarizes this loop.

Gaussian process + expected improvement → five-dimensional geometry
↓ checkpointed controller and timestamped CSV log
Stampede3 wrapper (36 MPI ranks) → **3-D MEEP + Harminv**
↓ return Q, update optimizer, serialize checkpoint

Fig. 1. Checkpointed Bayesian–FDTD optimization workflow.

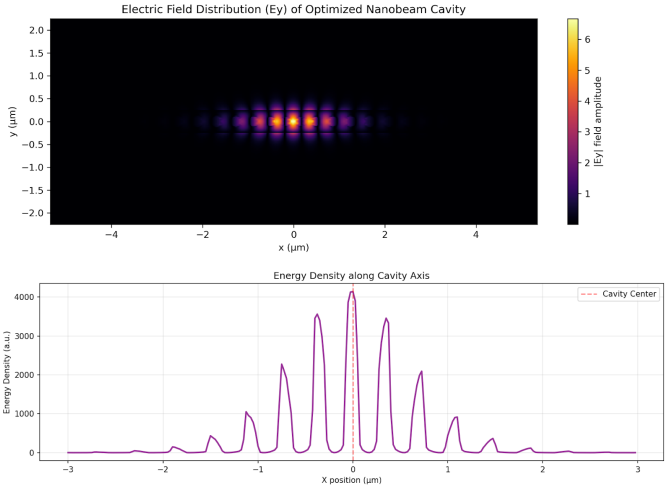


Fig. 2. Field characterization of the selected cavity. Top: simulated E_y distribution in the cavity plane. Bottom: axial electric-energy-density profile, showing localization near the defect center and decay into the mirror sections.

III. Electromagnetic Evaluation

Search-stage geometries were evaluated with three-dimensional MEEP FDTD at 40 pixels/μm using a nondispersive silicon index of 3.45, a broadband E_y-polarized Gaussian source, perfectly matched layers, and mirror symmetries in y and z [5]. Harminv monitors sampled the cavity center and nearby points, and the largest extracted quality factor was returned as the Bayesian objective.

The selected geometry was subsequently evaluated at 60 pixels/μm with a larger longitudinal domain, five Harminv sampling locations, and discrete-Fourier-transform field monitors. Additional propagation time allowed broadband transients to leave the sampled region before field extraction. The normalized mode-volume estimate $\widetilde{V}$ was calculated from the ratio of integrated to peak sampled electric-energy density. Silicon overlap was calculated as the fraction of sampled electric energy in cells with dielectric constant greater than two. Equation (1) then supplied the ideal geometric Purcell estimate.

IV. Results and Quantum-Photonic Relevance

The terminal focused stage identified $a_{\mathrm{start}} = 0.41382$ μm, $a_{\mathrm{end}} = 0.33957$ μm, $p = 1.08276$, $N_{\mathrm{def}} = 5$, and $s_{\mathrm{cav}} = 0.14912$ μm. The retained search record gives $Q = 2.46304\times10^7$ for this geometry. Table I reports the field-derived quantities.

The E_y map in Fig. 2 is centered within the defect and decays through the mirror region, while the silicon overlap indicates that most sampled electric energy remains in the dielectric. For a compatible solid-state emitter placed and tuned near the field maximum, a cavity with large $Q/\widetilde{V}$ could increase emission into a selected optical mode and thereby support more efficient spin–photon or emitter–photon interfaces for chip-scale quantum networking [1]. The present simulation does not demonstrate a qubit, a deterministic single-photon source, or strong coupling. Those claims require emitter-specific coupling and decoherence rates, linewidth, detuning, and dipole alignment.

TABLE I
Selected Simulated Cavity Metrics

Quantity	Value
Taper exponent, p	1.08276
Quality factor, Q	2.46304×10^7
Estimated normalized mode volume, $\widetilde{V}$	0.38461
Ideal geometric Purcell estimate	4.86212×10^6
Silicon electric-energy overlap	90.762%

The search establishes a high-performing candidate in a jointly optimized sub-quadratic region. Because all five variables changed during optimization, the data do not isolate p as the sole cause of the improvement. A matched ablation replacing $p = 1.08276$ with $p = 2$ while holding the other coordinates fixed is therefore a priority. Further validation should include grid and domain convergence, fabrication-disorder and material-loss models, an independently reproduced mode-volume calculation, and experimental optical characterization.

V. Conclusion

A checkpointed Bayesian controller, a Stampede3 MPI wrapper, and a parallel MEEP solver identified a near-linear taper with $Q = 2.46304 \times 10^7$ and estimated normalized mode volume $\widetilde{V} = 0.38461$. The cavity is a candidate for future solid-state quantum-emitter interface studies, and preserves optimization campaigns across scheduled HPC sessions.

Acknowledgment

The authors thank Patrick Flanigan of North Carolina Central University for TACC access and initial guidance in nanophotonics and MEEP, and TACC for computational resources provided. OpenAI ChatGPT (GPT-5.5 Thinking) assisted with organization and language revision [6].

References

[1] D. D. Awschalom, R. Hanson, J. Wrachtrup, and B. B. Zhou, "Quantum technologies with optically interfaced solid-state spins," *Nature Photon.*, vol. 12, pp. 516–527, 2018.

[2] J. D. Joannopoulos, S. G. Johnson, J. N. Winn, and R. D. Meade, *Photonic Crystals: Molding the Flow of Light*, 2nd ed. Princeton, NJ, USA: Princeton Univ. Press, 2008.

[3] Q. Quan and M. Lončar, "Deterministic design of wavelength scale, ultra-high Q photonic crystal nanobeam cavities," *Opt. Express*, vol. 19, no. 19, pp. 18529–18542, 2011.

[4] D. R. Jones, M. Schonlau, and W. J. Welch, "Efficient global optimization of expensive black-box functions," *J. Global Optim.*, vol. 13, no. 4, pp. 455–492, 1998.

[5] A. F. Oskooi, D. Roundy, M. Ibanescu, P. Bermel, J. D. Joannopoulos, and S. G. Johnson, "MEEP: A flexible free-software package for electromagnetic simulations by the FDTD method," *Comput. Phys. Commun.*, vol. 181, no. 3, pp. 687–702, 2010.

[6] OpenAI, "ChatGPT," GPT-5.5 Thinking, 2026. [Online]. Available: https://openai.com/chatgpt/overview/. Accessed: Jun. 26, 2026.